Geophysical Research Letters

RESEARCH LETTER
10.1029/2019GL086572

Jupiter's Gravity Field Halfway Through the Juno Mission

D. Durante[1], M. Parisi[2], D. Serra[3], M. Zannoni[4], V. Notaro[1], P. Racioppa[1], D. R. Buccino[2], G. Lari[3], L. Gomez Casajus[4], L. Iess[1], W. M. Folkner[2], G. Tommei[3], P. Tortora[4], and S. J. Bolton[5]

[1]Sapienza University of Rome, Rome, Italy, [2]Jet Propulsion Laboratory, California Institute of Technology, Pasadena, CA, USA, [3]University of Pisa, Pisa, Italy, [4]University of Bologna, Forlì, Italy, [5]Southwest Research Institute, San Antonio, TX, USA

Key Points:
- Juno updates Jupiter's gravity field halfway through its mission, revealing a largely axially symmetric, north-south asymmetric field
- Hints to a non-static and/or non-axially symmetric field, possibly related to several different physical mechanisms, appear in the data
- The tidal response is evaluated and compared to interior model predictions

Supporting Information:
- Supporting Information S1
- Data Set S1
- Data Set S2

Correspondence to:
D. Durante,
daniele.durante@uniroma1.it

Citation:
Durante, D., Parisi, M., Serra, D., Zannoni, M., Notaro, V., Racioppa, P., et al. (2020). Jupiter's gravity field halfway through the Juno mission. *Geophysical Research Letters*, *47*, e2019GL086572. https://doi.org/10.1029/2019GL086572

Received 9 DEC 2019
Accepted 28 JAN 2020
Accepted article online 3 FEB 2020

Abstract The Juno spacecraft reached the mid-point of its nominal mission in December 2018, after completing 17 perijove passes. Ten of these were dedicated to the determination of the gravity field of the planet, with the aim of constraining its interior structure. We provide an update on Jupiter's gravity field, its tidal response and spin axis motion over time. The analysis of the Doppler data collected during the perijove passes hints to a non-static and/or non-axially symmetric field, possibly related to several different physical mechanisms, such as normal modes or localized atmospheric or deeply-rooted dynamics.

Plain Language Summary Jupiter's gravity field has been updated with the use of Juno's data collected up to the mid-point of its mission. The field is largely symmetric about the rotation axis, and shows conspicuous north-south asymmetry. Possible non-static and/or non-axially symmetric field is compatible with the data.

1. Introduction

The Juno spacecraft has been orbiting Jupiter since 4 July 2016, completing perijove passes (PJ) once every 53 days. The mid-point of Juno's nominal mission has been reached after the 17th pass at perijove, PJ17, on 21 December 2018. In that timeframe, 10 perijove passes have been dedicated to the determination of Jupiter's gravitational field by exploiting extremely accurate Doppler measurements enabled by Juno's radio tracking system. The gravity science experiment has been successful in measuring Jupiter's gravity field (Folkner et al., 2017; Iess et al., 2018), whose interpretation revealed crucial information about Jupiter's interior. Wahl et al. (2017) suggested the presence of a diluted core, with heavy elements extended up to half of Jupiter's radii, in agreement with formation models (Liu et al., 2019). The north-south asymmetry of Jupiter's gravity field has been tied to surface zonal winds extending down to a few thousands of kilometers (Kaspi et al., 2018), revealing a substantial mass involvement, while the deep interior nearly rotates as a rigid body (Guillot et al., 2018).

We present an update of Jupiter's gravity field and tidal response when Juno is halfway through its nominal mission. The increased number of orbits, designed to sample Jupiter at uniform longitudinal intervals, allows for a better characterization of the gas giant. In addition, since Juno sampled the tidal bulge at different locations (see Figure S1 in Supporting Information), the gravitational tidal response to the Galilean satellites can be measured.

2. Observation geometry and data

Juno's orbits have been designed to avoid Jupiter's intense radiation belts. Being in a highly eccentric, polar orbit, Juno passes very close to Jupiter's cloud level, at an altitude of approximately 3500 km (see Table 1), spanning latitudes from the North pole to the South pole in roughly 2 hours.

During Juno's close encounter with Jupiter, the radio science investigation exploits Doppler shift measurements to determine the spacecraft orbit and Jupiter's gravity field. In a typical gravity pass, the Deep Space Station (DSS) 25 antenna, located in the Goldstone complex of NASA's Deep Space Network, simultaneously transmits both X-band (7.2 GHz) and Ka-band (34 GHz) radio signals. These signals are transmitted back preserving phase coherency by the on-board SDST (Small Deep Space Transponder) and KaTS (Ka-band Translator System) respectively at X-band (8.4 GHz) and Ka-band (32 GHz). The dual-link configuration

Table 1
Summary of orbital geometry and tracking configuration. Latitude and longitude coordinates are given in System III; altitude is with respect to the oblate Jupiter. The angle between the Negative Orbit Normal (NON) and Earth's direction determines the projection of Juno's velocity along the line-of-sight. The Sun-Earth-Probe (SEP) angle dictates the plasma noise contribution to the radio links. The number of Doppler points is followed by the tracking station and the radio links' bands. The Root Mean Square (RMS) of the open loop Doppler points, converted to two-way range rate, is given for the perijove tracking pass only.

Perijove	Date of perijove (UTC)	Perijove lat. & lon.	Perijove altitude (km)	NON-to-Earth (°)	SEP (°)	Doppler points at 60 s and tracking configuration	RMS of perijove pass at 60 s (mm/s)
PJ01	27 Aug. 2016 12:50:44	3.8°, 264.2°	4162.8	2.8	22.6	457 (X/X+X/Ka, DSS 55)	0.106
PJ03	11 Dec. 2016 17:03:41	5.6°, 354.5°	4153.2	19.2	61.4	383 (X/X+Ka/Ka, DSS 25) + 275 (X/X, DSS 43)	0.018
PJ06	19 May 2017 06:00:43	8.7°, 220.2°	3501.6	15.1	135.5	457 (X/X+Ka/Ka, DSS 25) + 244 (X/X, DSS 43)	0.014
PJ08	1 Sep. 2017 21:48:50	10.4°, 41.0°	3500.5	23.4	42.7	417 (X/X+Ka/Ka, DSS 25) + 87 (X/X, DSS 43)	0.016
PJ10	16 Dec. 2017 17:57:38	10.5°, 64.1°	4276.9	45.5	40.7	360 (X/X+Ka/Ka, DSS 25) + 247 (X/X, DSS 43)	0.019
PJ11	7 Feb. 2019 13:51:49	12.2°, 154.6°	3468.9	53.2	86.8	361 (X/X+Ka/Ka, DSS 25) + 120 (X/X, DSS 36)	0.011
PJ13	24 May 2018 05:39:50	14.8°, 335.9°	3497.9	48.2	163.4	391 (X/X+X/Ka, DSS 26) + 159 (X/X, DSS 43)	0.024
PJ14	16 Jul. 2018 05:17:22	15.7°, 291.5°	3498.0	45.3	109.7	385 (X/X+Ka/Ka, DSS 25) + 357 (X/X, DSS 43)	0.018
PJ15	7 Sep. 2018 01:11:40	15.6°, 22.0°	3499.2	49.8	63.6	334 (X/X+Ka/Ka, DSS 25) + 323 (X/X, DSS 43)	0.030
PJ17	21 Dec. 2018 16:59:48	18.1°, 156.6°	5053.3	70.8	20.2	43 (X/X, DSS 55) + 309 (X/X+Ka/Ka, DSS 25) + 127 (X/X, DSS 43)	0.026

allows the calibration of about to 75% of dispersive effects affecting the radio link (Bertotti et al., 1993; Mariotti & Tortora, 2013). During PJ01 and PJ13, a common X-band uplink was retransmitted by Juno's SDST in both X- and Ka-band, which only allows for the removal of the dispersive noise affecting the downlink leg, thus limiting the data quality improvement.

For each observation arc, Goldstone complex's data enclose the perijove epoch. In addition, the dataset includes measurements acquired at the Canberra DSN complex, just after Goldstone's antenna completed the tracking pass (see Table 1 for tracking configuration). These additional data are less accurate since only an X-band link is established, and plasma noise is an important noise source at small Sun-Earth-Probe angles (Asmar et al., 2005). However, the post-perijove pass provides additional constraints on Juno's trajectory, allowing a modest decrease of the uncertainties in gravity coefficients and tides (at most 20%). Since Juno performs a large orbit trim maneuver 7.5 hours after the perijove pass, data collected afterwards are irrelevant in the gravity field retrieval, and thus have not been used.

In addition to Doppler data, the ground stations collect regularly range data as well, and VLBI upon request (Jones et al., 2019). These data do not provide significant information on Jupiter's gravity field but constrain the location of the Jovian system in the Solar System. The latest available planetary ephemerides (Folkner & Park, 2018) are sufficiently accurate in locating the Jovian system with respect to the Earth, thus range data have not been included in our solution but used to assess its stability.

2.1. Data acquisition and calibration

An open loop receiver recorded the received electric field at 1 kHz, while a software phase-locked loop generated the Doppler shifts every 1 s. The data have been compressed to 60 s, allowing sufficient sampling of the gravity signal of interest. The Allan deviations of the plasma-calibrated Doppler residuals are roughly consistent with white frequency noise.

The path delay fluctuations induced by Earth's troposphere have been calibrated using the Advanced Water Vapor Radiometer available at DSS 25, which enables an improvement of up to 30% in total noise with respect to using standard calibration data (a combination of GPS and meteorological data).

During a perijove pass, the radio link crosses the Io plasma torus (Phipps & Withers, 2017), a belt of charged particles resulting from Io's volcanic activity. The dual-link configuration effectively suppresses this contribution. During PJ01 and PJ13, only the downlink dispersive contribution can be extracted. The uplink signal is calibrated by assuming that, being Juno close to the torus, the dispersive contribution is that of the downlink, after appropriate scaling for the different frequency.

3. Methods

The Doppler data have been analyzed with two independent software packages, providing consistent results: JPL's latest orbit determination software, MONTE (Evans et al., 2018), and ORBIT14, developed at University of Pisa, Italy (Serra et al., 2016; Serra et al., 2019). The dynamical model of Juno includes all the known effects which contribute significantly to the motion of Juno about Jupiter, as in Iess et al. (2018): the gravitational accelerations of the Solar System planets, Jupiter's Galilean satellites, Amalthea, and Thebe, in a relativistic framework; Jupiter's non-spherical gravitational field, expanded in spherical harmonics; tides raised on Jupiter by the Sun and the Galilean satellites; Jupiter's spin axis motion; the relativistic Lense-Thirring precession; the solar radiation pressure on Juno; Jupiter's albedo and thermal emission; Juno's repointing turns.

However, reducing the data to the noise level in a combined fit of 10 perijove passes requires the inclusion of small empirical accelerations acting on Juno. The same approach has been adopted by Iess et al. (2019) in the analysis of Cassini's Grand Finale Doppler data for the determination of Saturn's gravity field. These accelerations, of unknown origin, may be related to–a combination of–several different physical mechanisms, all plausible (see Section 4.3). The use of empirical accelerations in the dynamical model has been preferred since the physical mechanism at play cannot be identified with our limited dataset. Also, we still cannot completely rule out unknown instrumental effects, not related to Jupiter's gravity.

Doppler observables are computed by solving the relativistic light-time equation, with a correction due to Jupiter's oblateness. We correct for the instrumental delays introduced at DSS 25, accurately characterized by Buccino et al. (2019). The observation model corrects for the phase-wrapping caused by Juno's own rotation (Marini, 1972). Thermal effects in the proximity of Jupiter cause an increase of Juno's solar panels temperature. Durante (2019) showed that the resulting bending of the panels is too small to affect the data analysis. In addition, the anisotropic thermal emission acceleration caused by the difference in temperature between the front and back sides of the panels is also negligible, being at most $2\text{x}10^{-10}$ m/s^2, ten times smaller than solar radiation pressure.

The data have been fitted using a multi-arc least square filter. For each arc, we solve for: Juno's initial position and velocity; a scale factor for solar radiation pressure; empirical accelerations acting on a 2-hour window centered on the perijove with a time update of 10 minutes, constant in Juno's RTN frame (defined by the radial, transverse, normal directions in Juno's osculating orbit); the instantaneous velocity change during Earth repointing turns. Parameters common to each arc are: Jupiter's gravitational parameter, GM; Jupiter's zonal gravity coefficients to degree 30 and non-zonal coefficients of degree 2; tidal Love numbers up to degree and order 4; Jupiter's spin axis motion, described by a constant and linear term in right ascension and declination.

Solar System ephemerides are given by JPL's release DE438 (Folkner & Park, 2018), which have been fitted to the first 1.5 years of Juno's range data. The accuracy of Jupiter's ephemeris is highly improved, and we do not adjust the position of the system's center of mass, as it was done in Iess et al. (2018). The ephemerides of Jupiter's satellites are given by Jup310 (Jacobson, 2009).

The tidal interactions between Jupiter and its satellites are important to understand the interior of the planet. We solve for the Love numbers of even $l - m$ (l: degree; m: order) up to degree and order 4 (the k_{lm} with odd $l - m$ are not observable due to the negligible inclination of Jupiter's satellites orbits), but fixed the value of the k_{l0} coefficients to model prediction (not observable due to the large correlation with zonal coefficients, J_l). We impose the same Love number for all the satellites, although static models of Jupiter predict small deviations between the Galilean satellites, due to Jupiter's large oblateness (Nettelmann, 2019; Wahl et al., 2016). An attempt to solve for satellite-dependent Love numbers has been made, but large correlations

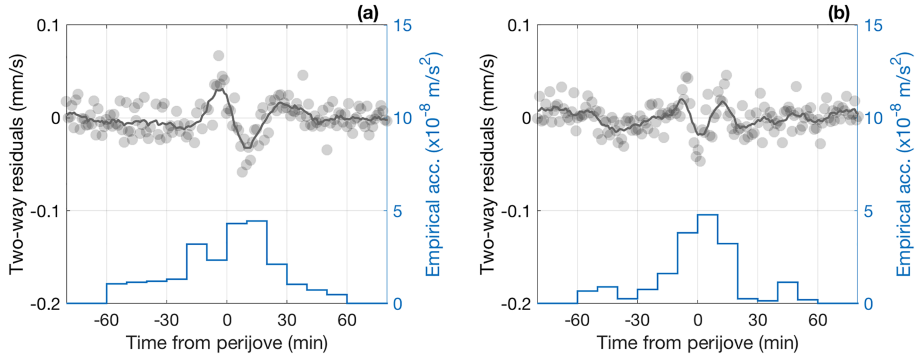

Figure 1. Estimated magnitude of empirical accelerations (blue line) and two-way Doppler residuals (black dots) if we do not include them, for (a) PJ03 and (b) PJ10 (see Figure S2 for all the perijoves). The light black line is a moving average of the residuals highlighting signatures near perijove.

prevent reliable estimates: the angle between Io and Europa is almost constant (it slowly increases from -14° to 30°) due to a resonance of Juno's period with Europa's period (Notaro et al., 2019).

The a priori uncertainties for the empirical accelerations have been selected according to the magnitude of the Doppler signatures when these accelerations were neglected: we observed a residual signal up to 0.1 mm/s (peak-to-peak) over a timescale of 10–15 minutes (see Figure 1), which corresponds to accelerations up to 10^{-7} m/s^2. We adopted an a priori uncertainty of $2\text{x}10^{-8}$ m/s^2 for the three components of the acceleration, which is the minimum level required to fit the data. Note that Iess et al. (2019) had to adopt an a priori value of $4\text{x}10^{-7}$ m/s^2 on Cassini's empirical accelerations to fit Doppler data from Grand Finale passes, a value 20 times larger.

4. Results

The gravity field coefficients are reported in Table 2. The central values are compatible with the solution reported in Iess et al. (2018), with uncertainties a factor of 2 to 8 smaller for low degree harmonics, and limited improvement on higher degrees (see Figure S3). The spherical harmonics coefficients of degree higher than 12 cannot be determined (the values are below the uncertainty) because of the large correlations with higher-degree coefficients caused by Juno's preferential sampling of the northern hemisphere.

Figure 2 shows Jupiter's reconstructed gravity anomalies along with their uncertainties. We removed the contributions from J_2, J_4, J_6 and J_8, which dominate the gravity signal due to Jupiter's fast rotation. Juno's ground tracks show the broad sampling in longitude obtained halfway through Juno's mission. The gravity signal appears to be symmetric about the rotation axis to great extent, with very limited longitudinal variation (see below Section 4.3 for further discussions).

As first discussed in Iess et al. (2018), the gravity field of Jupiter is north-south asymmetric, with a strong correlation with the zonal wind profile, as expected from thermal wind balance (Kaspi et al., 2018). The location of the large gravitational signals coincides with Jupiter's North Equatorial Belt and North Temperate Belt (between 20 °N and 30 °N), where the latitudinal wind gradient is the largest.

In terms of uncertainties, Juno's sampling in latitude is highly uneven due to the elliptical orbit. The latitudinal profile of gravity anomalies has an uncertainty (3-σ) smaller than 0.1 mGal in the limited region from 5 to 15 °N; smaller than 1 mGal in the broader region from 25 °S to 50 °N. The gravity anomalies (Figure 2, left panel) have been limited to the region where the uncertainty is smaller than the value. At the poles, the uncertainties reach up to 1 Gal, thus the recovered anomaly is not reliable.

4.1. Spin and principal axes

The motion of Jupiter's rotation axis has been solved as part of the fitting process. We estimated the initial position at 1 Jan. 2017 12:00 TDB and a linear rate in the plane of the sky. Figure 3 compares the estimated location of the spin axis at the time of the perijoves with the latest IAU model (Archinal et al., 2018), determined by integrating the torques exerted by Jupiter's main satellites and the Sun and fitted to earlier

Table 2
*Gravity field unnormalized coefficients and tidal Love numbers. The reference radius is 71492 km. The value for J_2 includes a tidal contribution currently estimated to be 6.72x10^{-8} from interior model predictions. The uncertainties are 3-σ. *Io's Love numbers for a satellite-dependent tidal model.*

	Value	Uncertainty
GM	126686534.1 km^3/s^2	8.4 km^3/s^2
J_2 (x10^6)	14696.5735	0.0017
C_{21} (x10^6)	0.0015	0.0023
S_{21} (x10^6)	0.0017	0.0015
C_{22} (x10^6)	0.0004	0.0011
S_{22} (x10^6)	0.0007	0.0010
J_3 (x10^6)	-0.0450	0.0033
J_4 (x10^6)	-586.6085	0.0024
J_5 (x10^6)	-0.0723	0.0042
J_6 (x10^6)	34.2007	0.0067
J_7 (x10^6)	0.120	0.012
J_8 (x10^6)	-2.422	0.021
J_9 (x10^6)	-0.113	0.036
J_{10} (x10^6)	0.181	0.065
J_{11} (x10^6)	0.016	0.111
J_{12} (x10^6)	0.062	0.190
k_{22}	0.565	0.018 (0.074*)
k_{31}	0.248	0.046 (0.171*)
k_{33}	0.340	0.116 (0.181*)
k_{42}	1.289	0.189 (1.059*)
k_{44}	0.546	0.406 (0.493*)

observations (Jacobson, 2002). Numerical simulations show that a linear model fits the non-linear IAU model over the limited time span of the current dataset without biasing the gravity estimates. However, the addition of future passages will require a more complete model.

The precession rate of Jupiter's spin axis is inversely proportional to the normalized Moment of Inertia (MoI), which in turn depends on the interior structure. A more accurate measurement of Jupiter's spin axis motion will be possible at the end of Juno's mission (Le Maistre et al., 2016), allowing an accurate determination of Jupiter's MoI, which could further constrain interior models (Helled et al., 2011).

Jupiter's spin axis is supposed to be perfectly aligned with Jupiter's pole direction, but principal axes can be misaligned. For a rigid body, the degree-2 gravity coefficients can be used to infer the directions of the principal axes of the body. However, the applicability of the classic formulas to gas giants remains unclear due to the large mass motion involved in the upper layers (about 1% of the total mass; Kaspi et al., 2018). The tilt of Jupiter's polar axis of inertia, in the limit of small rotations and negligible equatorial flattening, is given by $\epsilon_x = S_{21}/J_2$ and $\epsilon_y = -C_{21}/J_2$ (rotations about the x and y axes, respectively). No statistically significant deviation from the spin axis has been observed yet, at the level of tens of milliarcseconds. At the surface, this corresponds to about 5 meters (assuming a polar radius of 66854 km).

The small values of C_{22} and S_{22}, which determine the equipotential shape of Jupiter's equator, allow a deviation from a circular shape by no more than half a meter.

4.2. Tidal response

The tidal response of Jupiter to the Galilean satellites and the Sun is described by means of Love numbers, whose estimates are reported in Table 2. The Love numbers k_{22} and k_{42} are well determined, with a relative uncertainty of 3% and 15%, respectively. The inclusion of additional data allows a 3-fold improvement in k_{22}'s uncertainty with respect to the solution given by Iess et al. (2018), and the first determination of k_{42}.

Our tidal model imposes an identical response of Jupiter to all the satellites, whereas theoretical models predict slightly different values according to the satellite, with the largest deviation seen in k_{42} (Wahl et al., 2016; Nettelmann, 2019). However, since the largest tidal deformation is induced by Io, we can compare our estimates, at first order, with Jupiter's interior model predictions for a static response to Io. We found that our estimates for k_{22} and k_{42} are below Io's predictions, with deviations larger than the given uncertainties. The other Love numbers are in agreement. However, if we use the satellite-dependent tidal model

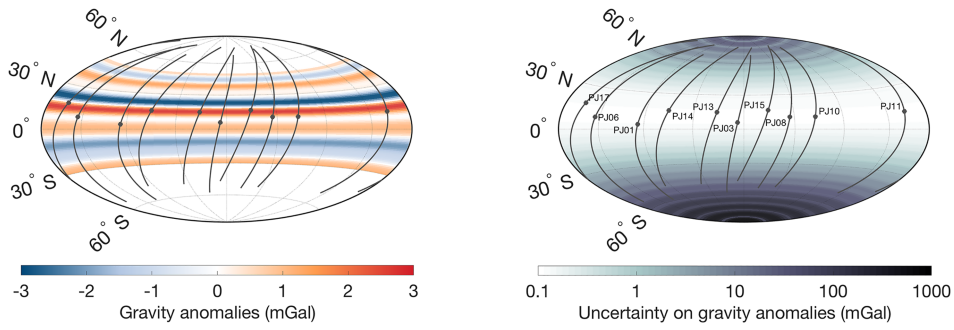

Figure 2. Gravity anomalies, their uncertainties, and ground tracks in System III. We removed the contribution of J_2, J_4, J_6 and J_8. The high latitudes are poorly sampled by Juno and not shown. The ground tracks cover 1 hour about the perijove (dots with labels).

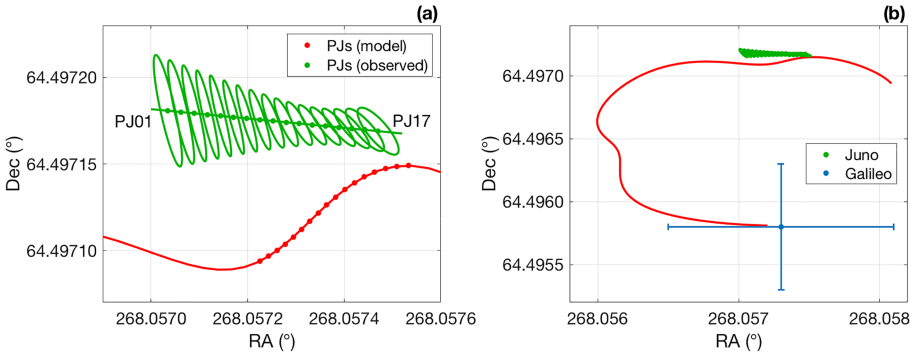

Figure 3. Jupiter's spin axis motion. (a) Green dots (ellipses) indicate the observed location (3-σ uncertainty) of the spin axis at the time of Juno's perijoves, to be compared with IAU model (red). (b) The model is compared with Juno's and Galileo's observations (Galileo's uncertainty is 1-σ).

(Notaro et al., 2019), without constraining our estimates, we obtain larger uncertainties: 0.074 for Io's k_{22} and 1.1 for Io's k_{42}, respectively a factor of 4 and 6 larger than our standard tidal model. The deviations from the static model values are below these uncertainties. Thus, we cannot conclude yet for an evidence of a deviation. Since interior model computations show that the static Love numbers are largely independent from reasonable interior model assumptions, any deviation would be important to characterize the dynamical contribution to the tidal response, which can be caused by resonances with internal normal modes.

4.3. Source of empirical accelerations

The inclusion of empirical accelerations is required to obtain a satisfactory fit of the Doppler data (Figure 1). The physical mechanisms for these accelerations may be related, but not restricted, to: gravitational effects caused by localized atmospheric wind dynamics (Galanti et al., 2017; Parisi et al., 2016), deeply seated gravity anomalies, possibly related to the magnetic field, Jupiter's normal modes (Durante et al., 2017), or a yet unknown instrumental effect. However, the identification of the phenomena at play from Juno's gravity data is nearly impossible due to the limited–both in time and in space–observations.

The empirical accelerations can potentially mimic either a time-dependent gravity field (normal modes) or longitude-dependent gravity anomalies (atmospheric or deeply-rooted wind dynamics). Being empirical, the recovered accelerations cannot be directly related to a physical phenomenon. Additionally, we tested different physical phenomena to check whether these were compatible with the data. We found that we obtain a fit by: (1) accounting for Jupiter's normal modes; (2) assuming a non-zonal field rotating at Jupiter's magnetic field rate; (3) including the localized gravity anomalies. These solutions are statistically consistent with our reference solution based on empirical accelerations.

Normal modes on gas giants have been observed both on Jupiter, through ground-based observations (Gaulme et al., 2011), and on Saturn, through analysis of Cassini ring occultation data (Hedman & Nicholson, 2013). Unfortunately, ground-based observations of Jupiter did not give constraints on the low radial order, fundamental (f-)modes, which are expected to dominate the gravity perturbations. It can be shown that the Doppler data can be explained by several different combinations of pressure or gravity modes (f-, p-, or g-modes) with values for the time-varying zonal coefficients $\widetilde{J}_{l,n}$ (l: degree, n: radial order) no smaller than roughly $5\text{x}10^{-10}$ (not constraining the frequency spectrum). This value is compatible with the expectations of Durante et al. (2017), when the energy for low-frequency modes was extrapolated by assuming the ratio of the amplitudes of p-modes and f-modes observed in the Sun.

Atmospheric dynamics proved suitable to explain the north-south asymmetry of Jupiter's gravity field; localized features, i.e., vortices, can potentially produce detectable gravity anomalies (Galanti et al., 2017). A gravity signal can also arise from deeply-rooted density anomalies, possibly related to Jupiter's magnetic field (e.g., Kong et al., 2016). Our analysis shows that a static tesseral field of at least degree and order 6 can explain the residual signal in Juno's Doppler data. These non-zonal gravity anomalies are of the order of 0.1 mGal, with comparable uncertainties, and would correspond to meridional winds extending down by no more than a few hundreds of kilometers.

5. Conclusions

We provided a mid-term update on Jupiter's gravity field. Our results are in good agreement with previous estimates and provide new clues about the gravity field of the gas giant planet.

The gravity anomalies are largely symmetric about the rotation axis, and strongly north-south asymmetric after removing the effect of the uniform rotation: Jupiter's gravity field is shaped by its fast rotation and perturbed by the surface zonal jets. Smaller contributions from several, yet indiscernible, physical phenomena are possible. These include Jupiter's normal modes, deeply rooted density anomalies, or atmospheric vortices.

The accuracy in determining the tidal response of Jupiter has improved, providing Love numbers up to degree and order 4. The Love number k_{22} and k_{42} have been accurately determined (in the limit of satellite-independent response), hinting at small deviations from the static value. Dynamical contributions can characterize Jupiter's normal modes which resonate with the tidal perturbations, providing further constraints on the internal structure of the gas giant.

Acknowledgments
This research was carried out at Sapienza University of Rome, University of Bologna, and University of Pisa under contract 2017-40-H.0 with the Italian Space Agency; at the Jet Propulsion Laboratory, California Institute of Technology, and the Southwest Research Institute under contract with NASA. All authors thank the Juno Interior Working Group for many fruitful discussions and continuous exchange of ideas. The data are available through NASA's Planetary Data System (Buccino, 2016).

References

Archinal, B. A., Acton, C. H., A'Hearn, M. F., Conrad, A., Consolmagno, G. J., Duxbury, T., et al. (2018). Report of the IAU Working Group on Cartographic Coordinates and Rotational Elements: 2015. *Celestial Mechanics and Dynamical Astronomy*, *130*(3), 1–46. https://doi.org/10.1007/s10569-017-9805-5

Asmar, S. W., Armstrong, J. W., Iess, L., & Tortora, P. (2005). Spacecraft Doppler tracking: noise budget and accuracy achievable in precision radio science investigations. *Radio Science*, *40*, RS2001. https://doi.org/10.1029/2004RS003101

Bertotti, B., Comoretto, G., & Iess, L. (1993). Doppler tracking of spacecraft with multi-frequency links. *Astronomy and Astrophysics*, *269*, 608–616.

Buccino, D., Border, J., Volk, C., & Yang, O. (2019). Measurement of Station Delay at DSS-25. *The Interplanetary Network Progress Report*, *42-217*, 1–11.

Buccino, D. R. (2016). Juno Jupiter Gravity Science Raw Data Set V1.0, JUNO-J-RSS-1-JUGR-V1.0, NASA Planetary Data System. https://atmos.nmsu.edu/PDS/data/jnogrv_1001/

Durante, D. (2019). The effect of Juno's solar panel bending on gravity measurements. *Journal of Guidance, Control, and Dynamics*, *42*, 2694–2699. https://doi.org/10.2514/1.G004503

Durante, D., Guillot, T., & Iess, L. (2017). The effect of Jupiter oscillations on Juno gravity measurements. *Icarus*, *282*, 174–182. https://doi.org/10.1016/j.icarus.2016.09.040

Evans, S., Taber, W., Drain, T., Smith, J., Wu, H., Guevara, M., et al. (2018). MONTE: the next generation of mission design and navigation software. *CEAS Space Journal*, *10*(1), 79–86. https://doi.org/10.1007/s12567-017-0171-7

Folkner, W. M., Iess, L., Anderson, J. D., Asmar, S. W., Buccino, D. R., Durante, D., et al. (2017). Jupiter gravity field estimated from the first two Juno orbits. *Geophysical Research Letters*, *44*, 4694–4700. https://doi.org/10.1002/2017GL073140

Folkner, W. M., & Park, R. S. (2018). Planetary and lunar ephemeris file DE438, NASA Navigation and Ancillary Information Facility. Retrieved from https://naif.jpl.nasa.gov/pub/naif/generic_kernels/spk/planets/de438.bsp

Galanti, E., Durante, D., Finocchiaro, S., Iess, L., & Kaspi, Y. (2017). Estimating Jupiter's Gravity Field Using Juno Measurements, Trajectory Estimation Analysis, and a Flow Model Optimization. *The Astronomical Journal*, *154*, 2. https://doi.org/10.3847/1538-3881/aa72db

Gaulme, P., Schmider, F.-X., Gay, J., Guillot, T., & Jacob, C. (2011). Detection of jovian seis- mic waves: a new probe of its interior structure. *Astronomy and Astrophysics*, *531*, A104. https://doi.org/10.1051/0004-6361/20116903

Guillot, T., Miguel, Y., Militzer, B., Hubbard, W. B., Galanti, E., Kaspi, Y., et al. (2018). A suppression of differential rotation in Jupiter's deep interior. *Nature*, *555*(7695), 227–230. https://doi.org/10.1038/nature25775

Hedman, M. M., & Nicholson, P. D. (2013). Kronoseismology: Using density waves in Saturn's c ring to probe the Planet's interior. *The Astronomical Journal*, *146*, 12. https://doi.org/10.1088/0004-6256/146/1/12

Helled, R., Anderson, J. D., Schubert, G., & Stevenson, D. J. (2011). Jupiter's moment of inertia: A possible determination by Juno. *Icarus*, *216*, 440–448. https://doi.org/10.1016/j.icarus.2011.09.016

Iess, L., Folkner, W. M., Durante, D., Parisi, M., Kaspi, Y., Galanti, E., et al. (2018). The measurement of Jupiter's asymmetric gravity field. *Nature*, *555*(7695), 220–222. https://doi.org/10.1038/nature25776

Iess, L., Militzer, B., Kaspi, Y., Nicholson, P., Durante, D., Racioppa, P., et al. (2019). Measurement and implications of Saturn's gravity field and ring mass. *Science*, *364*, aat2965. https://doi.org/10.1126/science.aat2965

Jacobson, R. A. (2002). The orientation of the pole of Jupiter. *Bulletin of the American Astronomical Society*, *34*, 936.

Jacobson, R. A. (2009). Jupiter satellite ephemeris file Jup310, NASA Navigation and Ancillary Information Facility. Retrieved from https://naif.jpl.nasa.gov/pub/naif/generic_kernels/spk/satellites/jup310.bsp

Jones, D. L., Romney, J. D., Folkner, W. M., Park, R. S., Jacobs, C. S., & Dhawan, V. (2019). The First Two Years of Juno Spacecraft Astrometry with the Very Long Baseline Array. IEEE Aerospace Conference, Big Sky, MT, USA. https://doi.org/10.1109/AERO.2019.8742108

Kaspi, Y., Galanti, E., Hubbard, W. B., Stevenson, D. J., Iess, L., Guillot, T., et al. (2018). The extension of Jupiter's jet to a depth of thousands of kilometers. *Nature*, *555*(7695), 223–226. https://doi.org/10.1038/nature25793

Kong, D., Zhang, K., & Shubert, G. (2016). Using Jupiter's gravitational field to probe the Jovian convective dynamo. *Scientific Reports*, *6*, 23497. https://doi.org/10.1038/srep23497

Le Maistre, S., Folkner, W. M., Jacobson, R. A., & Serra, D. (2016). Jupiter spin-pole precession rate and moment of inertia from Juno radio-science observations. *Planetary and Space Science*, *126*, 78–92. https://doi.org/10.1016/j.pss.2016.03.006

Liu, S.-F., Hori, Y., Müller, S., Zheng, X., Helled, R., Lin, D., & Isella, A. (2019). The formation of Jupiter's diluted core by a giant impact. *Nature*, *572*(7769), 355–357. https://doi.org/10.1038/s41586-019-1470-2

Marini, J. (1972). A Test of the Effect of Satellite Spin on Two-Way Doppler Range- Rate Measurements. *IEEE Transactions on Aerospace and Electronic Systems*, *8*, 269–272. https://doi.org/10.1109/TAES.1972.309508

Mariotti, G., & Tortora, P. (2013). Experimental validation of a dual uplink multifrequency dispersive noise calibration scheme for deep space tracking. *Radio Science*, *48*, 111–117. https://doi.org/10.1002/rds.20024

Nettelmann, N. (2019). Tesseral harmonics of Jupiter from static tidal response. *Astrophysical Journal*, *874*, 2. https://doi.org/10.3847/1538-4357/ab0c03

Notaro, V., Durante, D., & Iess, L. (2019). On the determination of Jupiter's satellite-dependent tides with Juno gravity data. *Planetary and Space Science*, *175*, 34–40. https://doi.org/10.1016/j.pss.2019.06.001

Parisi, M., Galanti, E., Finocchiaro, S., Iess, L., & Kaspi, Y. (2016). Probing the depth of Jupiter's Great Red Spot with the Juno gravity experiment. *Icarus*, *267*, 232–242. https://doi.org/10.1016/j.icarus.2015.12.011

Phipps, P. H., & Withers, P. (2017). Radio occultations of the Io Plasma Torus by Juno are feasible. *Journal of Geophysical Research: Space Physics*, *122*, 1731–1750. https://doi.org/10.1002/2016JA023447

Serra, D., Dimare, L., Tommei, G., & Milani, A. (2016). Gravimetry, rotation and angular momentum of Jupiter from the Juno Radio Science Experiments. *Planetary and Space Science*, *134*, 100–111. https://doi.org/10.1016/j.pss.2016.10.013

Serra, D., Lari, G., Tommei, G., Durante, D., Gomez Casajus, L., Notaro, V., et al. (2019). A Solution of Jupiter's Gravitational Field from Juno Data with the ORBIT14 Software. *Monthly Notices of the Royal Astronomical Society*, *490*(1), 766–772. https://doi.org/10.1093/mnras/stz2657

Wahl, S. M., Hubbard, W. B., & Militzer, B. (2016). Tidal response of a preliminary Jupiter model. *Astrophysical Journal*, *831*, 14. https://doi.org/10.3847/0004-637X/831/1/14

Wahl, S. M., Hubbard, W. B., Militzer, B., Guillot, T., Miguel, Y., Movshovitz, N., et al. (2017). Comparing Jupiter interior structure models to Juno gravity measurements and the role of a dilute core. *Geophysical Research Letters*, *44*, 4649–4659. https://doi.org/10.1002/2017GL073160